Quantification of stiffness measurement errors in resonant ultrasound spectroscopy of human cortical bone

Xiran Cai, Laura Peralta, Pierre-Jean Gouttenoire, Cécile Olivier, Françoise Peyrin, Pascal Laugier, Quentin Grimal

Quantification of stiffness measurement errors in resonant ultrasound spectroscopy of human cortical bone

Xiran Cai,[1, a)] Laura Peralta,[1] Pierre-Jean Gouttenoire,[2] Cécile Olivier,[3, b)] Françoise Peyrin,[3, b)] Pascal Laugier,[1] and Quentin Grimal[1]

[1)] *Sorbonne Universités, UPMC Univ Paris 06, INSERM UMR-S 1146, CNRS UMR 7371, Laboratoire d'Imagerie Biomédicale, 15 rue de l'Ecole de Médecine, Paris 75006, France*

[2)] *ESRF, 71 Avenue des Martyrs, Grenoble 38043, France*

[3)] *Univ. Lyon, INSA-Lyon, Université Claude Bernard Lyon 1, CNRS, INSERM, CREATIS UMR 5220, U1206, 7 Avenue Jean Capelle, Villeurbanne 69621, France*

(Dated: October 6, 2017)

Measurement errors in resonant ultrasound spectroscopy

Resonant ultrasound spectroscopy (RUS) is the state-of-the-art method used to investigate the elastic properties of anisotropic solids. Recently, RUS was applied to measure human cortical bone, an anisotropic material with low Q-factor (20), which is challenging due to the difficulty in retrieving resonant frequencies. Determining the precision of the estimated stiffness constants is not straightforward because RUS is an indirect method involving minimizing the distance between measured and calculated resonant frequencies using a model. This work was motivated by the need to quantify the errors on stiffness constants due to different error sources in RUS, including uncertainties on the resonant frequencies and specimen dimensions and imperfect rectangular parallelepiped (RP) specimen geometry. The errors were firstly investigated using Monte-Carlo simulations with typical uncertainty values of experimentally measured resonant frequencies and dimensions assuming a perfect RP geometry. Secondly, the exact specimen geometry of a set of bone specimens were recorded by synchrotron radiation micro-computed tomography. Then, a 'virtual' RUS experiment is proposed to quantify the errors induced by imperfect geometry. Results show that for a bone specimen of $\sim 1^\circ$ perpendicularity and parallelism errors, an accuracy of a few percent ($< 6.2\%$) for all the stiffness constants and engineering moduli is achievable.

PACS numbers: PACS: XXXX

[a]Electronic mail: xiran.cai@upmc.fr; Corresponding author.

[b]Also at: ESRF, 71 Avenue des Martyrs, Grenoble 38043, France

I. INTRODUCTION

Bone adaptation in response to mechanical loading and the subsequent optimization of bone strength are regulated by mechanosensitive osteocytes, which are capable of sensing strain[1]. For a given load, bone stiffness determines the local strain, hence investigating bone stiffness in detail should allow gaining insight into bone functional adaptation mechanisms and bone strength.

As the structure of human cortical bone, like many natural materials, is hierarchical[2], it is necessary to investigate it at different scales. In particular, cortical bone elastic properties at the mesoscale (millimeter-scale) are of special interest as they depend on tissue properties at all the smaller length scales and have a direct impact on the mechanical behavior of bone at the macroscale[3,4]. In addition, this is the level at which cortical bone functions, in concert with the overall gross shape of a bone in resisting functional loads[5]. The mesoscopic level is also appropriate to investigate the regional variations of the elastic properties within a bone[6], which is necessary to refine finite element models to predict patterns of stress and strain. In this context, precise and practical measurement methods for assessing cortical bone elasticity at the mesoscale are needed.

In general, bone material can be considered as a transversely isotropic or orthotropic material, hence engineering moduli such as Young's moduli, shear moduli, and Poisson's ratio can be derived from the components of the stiffness tensor. Ultrasonic techniques are well suited to probe the anisotropic elastic properties of bone. The most widely used ultrasonic measurement method, which was introduced by Lang[7] and used by many research groups[8–14], consists in measuring the ultrasonic wave velocity (UWV). Despite its apparent simplicity, UWV measurements present several pitfalls that must be carefully considered. The final result can be affected by some factors, including the size of the measured specimen compared to the wavelength, the presence of heterogeneities, or the signal processing required to estimate the time of flight to calculate velocity[15,16].

Resonant ultrasound spectroscopy (RUS) has been recently introduced as an alternative technique to the measurement of human cortical bone stiffness[17]. RUS has been extensively used since 1990's to investigate the elastic properties of solids as diverse as piezoelectric materials[18], metallic alloys[19], metallic glasses[20] and composites[21], hard polymers[22], wood[23], and mineralized tissues[17,24,25] for applications ranging from theoretical physics to industrial problems. The main advantage of RUS, compared to other techniques such as UWV measurements and mechanical testing, is that the full set of the elastic tensor can be assessed non-destructively from a single measurement[26,27]. Briefly, in a RUS experiment, resonant frequencies of a free vibrating specimen are retrieved from the resonant spectrum measured by a pair of ultrasonic transducers. Then, the stiffness constants are adjusted using an iterative numerical procedure (inverse problem) until the calculated eigenfrequencies of a free vibration object (forward problem) match with the experimentally measured resonant frequencies.

Determining the precision of the different stiffness constants measured by RUS is not straightforward because RUS is an indirect method to obtain stiffness constants, involving the minimization of the distance between measured and calculated frequencies. Essentially, elasticity estimation errors arise from two sources[19,26] (1) the imperfectly measured resonant frequencies; and (2) inadequate geometry of the forward model. The latter is caused by possible shape imperfections (i.e., non perfectly parallel or perpendicular surfaces) not taken into account in the model, and metrological errors in the measurement of the specimen's dimensions.

The effects of RUS measurement errors have been addressed to some extent in several studies in the case of perfectly rectangular parallelepiped (RP) shaped specimen geometry[26,28–30]. Regarding the first source of error (imperfectly measured resonant frequencies), the uncertainties on the determined stiffness constants have been estimated using the perturbation theory (assuming perfect RP specimen geometry). By determining the sensitivity of the resonant frequencies to the stiffness constants, the uncertainties of the stiffness constants can be quantified as a function of the relative root mean square error (RMSE) σ_f expressing the misfit between the measured and calculated resonant frequencies[26,29]. For instance, Sedlack et al.[30] quantified the typical uncertainties measured on a silicon carbide ceramics parallelepiped specimen and found relative measurement errors of less than 0.35%, 0.80% and 2.80% for shear, longitudinal and off-diagonal stiffness constants respectively, for $\sigma_f = 0.25$ %. Regarding the second source of error (imperfect geometry), on an empirical basis, Migliori et al.[26,31] recommended that shape errors in parallelism and perpendicularity between faces should be limited to 0.1% in order to keep errors on stiffness constants within acceptable bounds, that is, close to 1%. However, there is no data in the open literature to support these numbers, as far as we know.

When measuring bone elasticity using RUS, errors on the measured resonant frequencies are larger compared to the case of other materials. This is related to the high viscoelastic damping of the material (Q-factor $\sim$ 20) resulting in resonant peaks overlapping and a lower accuracy of the measured frequencies compared to the case of high-Q materials[22,32]. In many RUS applications only a few specimens are measured, and much time is devoted to specimen's preparation in order to achieve an excellent geometrical quality. In contrast, the high variability of elastic properties in biological materials, in particular within a bone[33], implies that several tens of specimens should be measured in order to obtain representative values of stiffness. As a result, polishing each bone specimen in successive steps[31] to obtain a very high geometrical quality is not practicable. Hence, the question arises of the accuracy of the measured elasticity after a relatively simple preparation with a precision saw. To the best of our knowledge, no systematic study has been conducted about neither the effects of an imperfect specimen geometry on the elastic properties of cortical bone measured by RUS, nor the combined effects when resonant frequencies uncertainties are also considered.

The objective of this study is to quantify the experimental errors when measuring cortical bone elasticity with RUS. We take advantage of recent advances in RUS inverse problem to quantify sources of errors using Monte Carlo simulations. Namely, the step consisting in pairing measured frequencies and their calculated counterparts in the forward problem, previously achieved by an expert user with a trial-and-error method, was recently automated[34]. This allows an automated processing of RUS spectra which is a necessary condition for Monte Carlo analyses of error propagation. The following error sources are considered: (1) uncertainties on the measurement of frequencies; (2) uncertainties on the measurement of dimensions (assuming a perfect RP shape); (3) imperfect specimen geometry (deviation from a perfect RP). Although our primary focus is the application of RUS to measure bone, the methodology introduced in this work and the quantified errors are of general interest for the discussion of the precision and accuracy of RUS measurements of various materials.

Section II briefly recalls the theory of RUS, then Section III presents the specimens included in this study and their experimental measurements. Firstly, their elasticity is assessed by RUS and secondly, the geometry of the specimens is obtained from synchrotron radiation micro-computed tomography (SR-μCT) images. In Section IV, the effects of measurement uncertainties caused by both specimen dimensions and frequency errors, are investigated by Monte Carlo simulations. Section V investigates the errors associated to the deviation of the specimens's shape from a perfect RP. Here, the finite element method (FEM) is used to calculate resonant frequencies accounting for the actual shape of the specimen. Finally, results are discussed in Section VI.

II. RUS THEORY

RUS method is extensively described elsewhere[26,27]. Here we summarize the process as implemented in the present work. The determination of stiffness constants of the material constitutive of a specimen of RP shape consists of the following steps: (1) the resonant frequencies $\mathbf{f}^{exp}$ of the specimen are measured; (2) using $\mathbf{f}^{exp}$, the stiffness constants $\mathbf{C}_{ij}$ ($ij = 11, 33, 13, 44, 66$) are determined by solving an optimization problem, i.e., minimizing the objective function (Eq. (1))[26]:

$$F(\mathbf{C}_{ij}) = \sum_k \left(\frac{f_k^{exp} - f_k^{mod}(\mathbf{C}_{ij})}{f_k^{exp}} \right)^2 \tag{1}$$

where $\mathbf{f}^{mod}$ are simulated eigenfrequencies of a model of the specimen (forward problem) and k is the index of the eigenfrequency. In the optimization, the mass is assumed known, and the shape is assumed to be a perfect RP of known dimensions, collected in vector $\mathbf{dim}$. Frequencies $\mathbf{f}^{mod}$ are calculated with the Rayleigh-Ritz method (RRM), which is a semi-analytical method that yields the result in a fraction of a second on a modern desktop computer. In Eq. (1), the experimental and simulated frequencies are assumed to be paired. In the present work, pairing is done automatically in a Bayesian optimization strategy[34].

III. MEASUREMENTS

A. Specimens

Cortical bone specimens were harvested from the left femur of 18 human cadavers. The femurs were provided by the Départment Universitaire d'Anatomie Rockefeller (Lyon, France) through the French program on voluntary corpse donation to science. The tissue donors or their legal guardians provided informed written consent to give their tissue for investigations, in accord with legal clauses stated in the French Code of Public Health. Among the

18 donors, 11 were females and 7 were males ($50-95$ years old, 77 ± 12.3, mean±SD). The fresh material was frozen and stored at -20°C.

The samples were slowly thawed and then, for each femur, approximately a 10 mm thick cross section was cut perpendicular to the bone axis from the mid-diaphysis. The cross section was then cut into 4 pieces (Fig. 1a). Two of these pieces (lateral and medial) were then used to prepare a RP specimen. They were fixed on a stainless steel block (Fig. 1b) that has three mutually perpendicular faces. Without unmounting the specimen, the steel block was successively positioned on each of these three faces on a reference stage in order to cut with a water-cooled low-speed diamond wire saw (Model 3241, Well, Lyon, France) in three mutually perpendicular planes. From each donor, one or two RP shaped specimens were prepared, which led to a set of 23 specimens. The nominal specimen size was 3x4x5 mm^3 in radial (axis 1), circumferential (axis 2) and axial direction (axis 3), respectively, defined by the anatomic shape of the femoral diaphysis. All specimens were kept hydrated during sample preparation. The dimensions ($\mathbf{dim}^{exp}$) and mass (m^{exp}) of each specimen were measured by a digital caliper (precision ± 0.01 mm) and a balance (precision ± 0.1 mg), respectively.

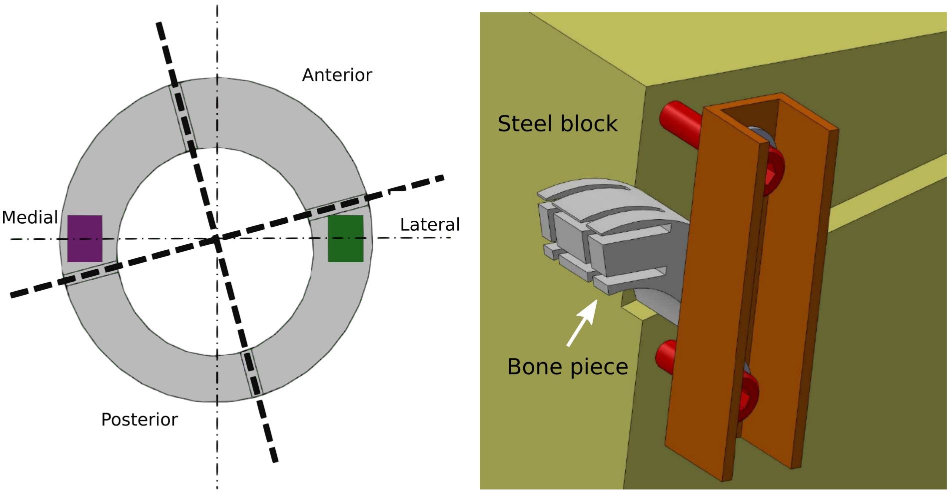

a) b)

Figure 1. a) the cross section of a femur was cut into 4 pieces according to the anatomical locations: lateral, medial, posterior and anterior; b) the steel block on which a bone piece was fixed for being cut by a diamond wire saw to retrieve a cuboid specimen. Two pairs of perpendicular cuts were realized by successively positioning the block on a reference stage with two mutually perpendicular faces.

B. Bone elasticity measurements by RUS

The experiments to measure the resonant frequencies and the numerical inversion to calculate the stiffness constants were performed following the RUS methodology specially adapted for bone and extensively presented elsewhere[17,34]. The procedure is briefly described as below. The bone specimen was placed on two opposite corners between two ultrasonic transducer (V154RM, Panametrics, Waltham, MA), one for emission and one for reception, to achieve a free boundary condition for vibration (Fig. 2).

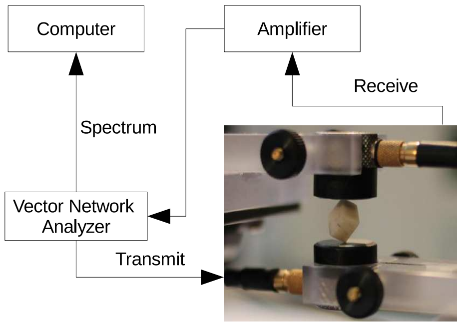

Figure 2. The RUS setup used in this study. A bone specimen is placed between two ultrasonic transducers at the two opposite corners to achieve a free boundary condition for vibration.

The frequency response of the vibration in a specified bandwidth, tuned so as to measure the 20-30 first resonant frequencies, was amplified by a broadband charge amplifier (HQA-15 M-10T, Femto Messtechnik GmbH, Berlin, Germany) and then recorded by a vector network analyzer (Bode 100, Omicron Electronics GmbH, Klaus, Austria). Six consecutive spectrum acquisitions were performed on each specimen at different orientations in order to maximize the number of detectable resonant frequencies. Then, the resonant frequencies were extracted from the spectra using the method dedicated to highly attenuative material[32] (Fig. 3).

Finally, assuming a transversely isotropic symmetry[12,35], the stiffness constants $\mathbf{C}_{ij}^{exp}$, were automatically calculated by solving the inverse problem formulated in a Bayesian framework[34](Sec. II). The prior information of the distribution of the stiffness constants, required for the Bayesian analysis, was taken from a previous study[13]. In the elastic tensor, $C_{12} = C_{11} - 2C_{66}$ and $(1-2)$ is the isotropy plane; C_{11} and C_{33} are the longitudinal stiffness constants, C_{12} and C_{13} are the off-diagonal stiffness constants and C_{44} and C_{66} represent the shear stiffness constants.

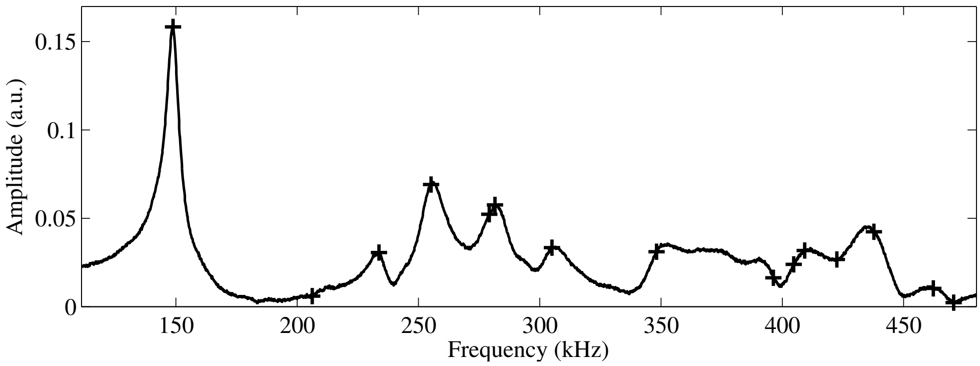

Figure 3. A typical resonant spectrum measured on a bone specimen. The plus signs (+) represent the extracted resonant frequencies.

C. Specimen geometry

The exact shape of the specimens and thus, deviation from the ideal RP shape was obtained using SR-μCT 3-D imaging, which was performed on the beamline ID19 at the European Synchrotron Radiation Facility (ESRF, Grenoble, France). This SR-μCT setup is based on a 3D parallel beam geometry acquisition[36,37]. The beam energy was tuned to 26 keV by using a (Si111) double crystal monochromator. A full set of 2D radiographic images were recorded using a CDD detector (Gadox scintillator, optic lenses, 2048 $\times$ 2048 Frelon Camera) by rotating the specimen in 1999 steps within a 360° range of rotation. The detector system was fixed to get a pixel size of 6.5 μm in the recorded images in which a region of interest of 1400x940 pixels was selected to fit the specimen.

For each specimen, the SR-μCT image (Fig. 4a) was reconstructed and binarized to get the bone phase. In RUS, the material of the measured specimen is considered as a homogeneous material. Here, the specimen is much larger than the representative volume element of continuum mechanics[4]. Accordingly, the vascular pores that are visible in the 3D image were filled up (Fig. 4b) using mathematical morphology operations to obtain a mask of each slice. Then the convex envelope of the bone masks was calculated and considered to be the exact shape of the specimen.

The quality of the geometry of the specimen was analyzed based on the reconstructed SR-μCT volume. The coordinates of the cloud of points of each specimen's face were collected and the equation of the planes fitting each face in the least-square sense were determined. The angles α and β between the normal of the planes were used to quantify the quality of the specimen's geometry compared to a perfect RP (Fig. 5). The perpendicularity errors

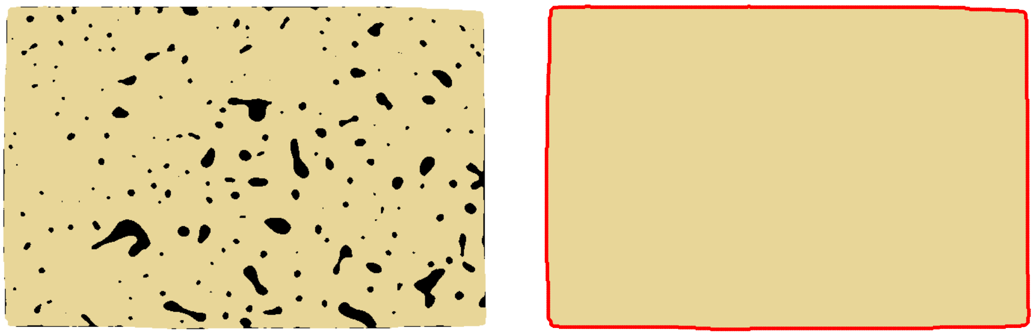

a) b)

Figure 4. a) A slice of the binarized image of bone structure. b) The mask of the bone slice after filling up the pores (the black parts in a)) and the contours (red color) detected from the mask. The contours of all the masks determine the external envelope of the specimen which was used to quantify its perpendicularity and parallelism quality.

between adjacent faces were quantified by $\delta\alpha = 90° - \alpha$. The parallelism errors between opposite faces were quantified by $\delta\beta = 180° - \beta$. The values of the angle errors for the 23 specimens (12 $\delta\alpha$ and 3 $\delta\beta$ per specimen) are collected in Fig. 6. The deviations (mean±std) from ideal perpendicularity and parallelism were -0.07°±0.85° and 0.30°±0.78°, respectively.

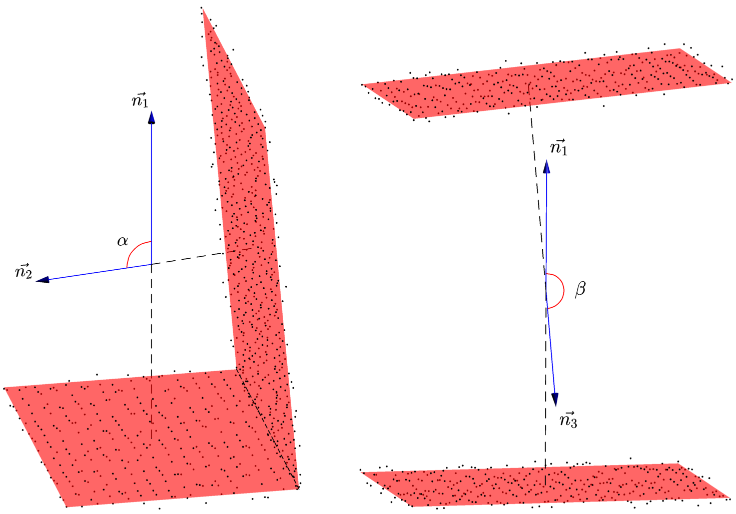

Figure 5. The angle α is defined by the angle between the normal ($\vec{n_1}$ and $\vec{n_2}$) of two adjacent faces which are found by fitting the cloud of points (the dots in the figures) with the equation of the best plane in the least-square sense; accordingly, β is defined by the angle between the normal ($\vec{n_1}$ and $\vec{n_3}$) of two opposite faces. For a perfect RP, α and β should equal to 90° and 180°, respectively.

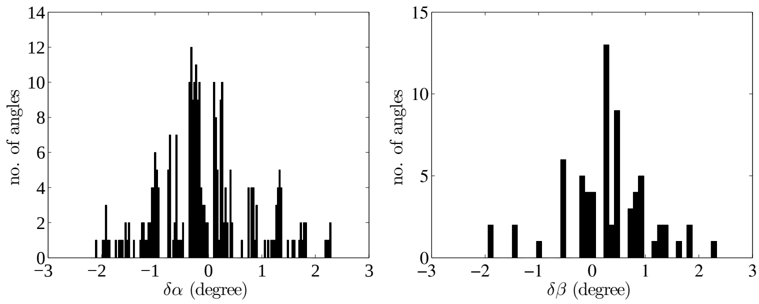

a) perpendicularity error $\delta\alpha$ b) parallelism error $\delta\beta$

Figure 6. The distributions of the perpendicularity error $\delta\alpha$ and parallelism error $\delta\beta$ of the 23 specimens.

IV. SIMULATION OF THE ERRORS DUE TO UNCERTAINTIES ON RESONANT FREQUENCIES AND DIMENSIONS

A. Method

We consider a perfect RP specimen as a reference, characterized by the dimensions $\mathbf{dim}^0$, mass m^0 and stiffness constants $\mathbf{C}^0_{ij}$ shown in Table I. In Table I, the values of $\mathbf{dim}^0$ are the mean values of the dimensions of the specimens used in this work. The value of m^0 was calculated assuming a typical mass density value of 1.87 mg/mm^3 taken as the mean value from a former study about human femoral cortical bone[13]. The values of $\mathbf{C}^0_{ij}$ correspond to the mean values of the stiffness of human femoral cortical bone at the mid-diaphysis[13]. The first 40 eigenfrequencies $\mathbf{f}^0$ of the reference specimen were calculated using the RRM. This number of frequencies was chosen according to the experimental frequency bandwidth in RUS measurements on human cortical bone specimens, which in practice contains approximately 40 resonant frequencies.

Table I. Properties of the reference RP bone specimen. The eigenfrequencies $\mathbf{f}^0$ of the reference specimens are associated to the parameters in this table.

$\mathbf{dim}^0$ (mm)	m^0 (mg)	$\mathbf{C}^0_{ij}$ (GPa)
$3 \times 4 \times 5$	112.2	19.58 29.04 11.74 5.83 4.28

In this section, Monte-Carlo simulations[38] were performed to quantify the propagation of the errors due to uncertainties on resonant frequencies and specimen dimensions. Repeated calculations of the stiffness constants were performed, each time randomly varying the input data (dimensions or/and resonant frequencies) within their stated limits of precision. Then we quantified the variability of each stiffness constant caused by dimension errors, by frequency errors, and by the association of both dimension and frequency errors.

The order of magnitude of the dimension error to be used in Monte-Carlo simulations was obtained comparing, for each specimen, the SR-μCT image with the dimensions $\mathbf{dim}^{exp}$ measured with the caliper. Specimen's dimensions obtained from the SR-μCT image are considered as a reference based on which the uncertainty of $\mathbf{dim}^{exp}$ can be estimated. In order to obtain a representative value ϵ of the dimension error, we compared, for each specimen the volume of the bone SR-μCT images and the volume of a hypothetical RP of dimensions $\mathbf{dim}^{exp} \pm \epsilon$. By equating these volumes for each of the 23 specimens and solving the equations, we obtained a series of values of ϵ shown in Fig. (7). The specimen's dimensions obtained from the SR-μCT image were found to be systematically smaller than $\mathbf{dim}^{exp}$. We choose the mean value of $\epsilon \approx 0.04$ mm as a conservative value to represent the accuracy of the dimensions measured by caliper. Accordingly, the uncertainty of $\mathbf{dim}^{exp}$ was set to 0.04 mm.

The standard error on the measured resonant frequencies used in Monte-Carlo simulations was chosen to be 0.5%, which is typically the repeatability of the measured resonant frequencies in bones[17].

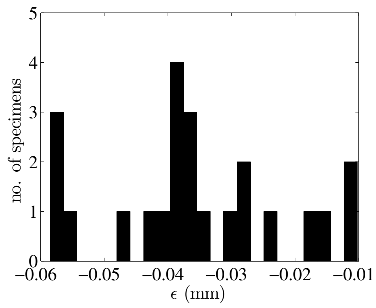

Figure 7. The distribution of the dimension error ϵ obtained by comparing for each specimen the volume of the bone SR-μCT reconstruction and the volume of a hypothetical RP of dimensions $\mathbf{dim}^{exp} \pm \epsilon$.

1. *Effects of uncertainties on dimension*

To quantify the effects of imprecise dimension measurements, 1000 random realizations of dimensions were generated from independent normal distributions centered on $\mathbf{dim}^0$ with a standard deviation of 0.04 mm, $\mathbf{dim}^p \sim N(\mathbf{dim}^0, 0.04^2)$. The number of random realizations was chosen following preliminary convergence tests. For each realization p, the stiffness constants $\mathbf{C}_{ij}^p$, were obtained by solving the inverse problem using $\mathbf{f}^0$ as proxy for experimental frequencies, and the frequencies $\mathbf{f}^p$ calculated for the inadequate forward model: specimen of perfect RP shape with uncertain dimensions $\mathbf{dim}^p$. The mass used in the forward model is that of the reference RP specimen (Table I). The inverse problem uses the objective function defined in Eq. (2). The stated input parameters for the simulation are summarized in Fig. 8 (block D).

$$F(\mathbf{C}_{ij}^p) = \sum_k \left(\frac{f_k^0 - f_k^p(\mathbf{C}_{ij}^p)}{f_k^0} \right)^2 \tag{2}$$

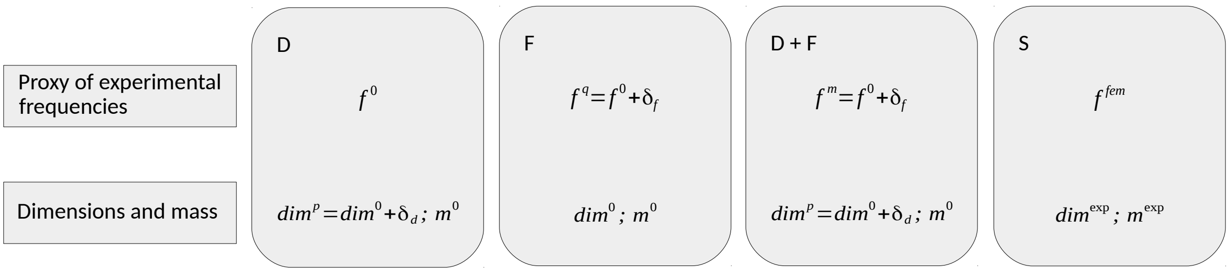

Figure 8. The input parameters for the simulations detailed in Secs. IV and V for quantifying stiffness estimation errors due to the experimental error sources: dimensions imprecision (block D), frequencies imprecision (block F), dimensions and frequencies imprecision (block D + F) and the imperfect specimen geometry (block S). δ_d and δ_f represent the deviations from the reference values dim^0 and f^0, respectively, that are randomly generated for each realization. Given dimension and mass are the constants used for the forward model.

2. *Effects of uncertainties on frequencies*

In a similar way, for the analysis of frequency imprecision, 1000 random realizations of frequencies from a normal distribution centered on $\mathbf{f}^0$ were generated assuming a relative standard deviation of 0.5%, $\mathbf{f}^q \sim N\left(\mathbf{f}^0, (0.005\mathbf{f}^0)^2\right)$. The number of random realizations was chosen following preliminary convergence tests. The stiffness constants $\mathbf{C}_{ij}^q$, were then obtained by solving the inverse problem based on the objective function (Eq. (3)) using $\mathbf{f}^q$ as proxy for experimental frequency values with an error and $\mathbf{f}^r$ calculated using $\mathbf{dim}^0$, m^0 and assuming a perfect RP specimen (Table I). The input parameters are summarized in Fig. 8 (block F).

$$F(\mathbf{C}_{ij}^q) = \sum_k \left(\frac{f_k^q - f_k^r(\mathbf{C}_{ij}^q)}{f_k^q} \right)^2 \tag{3}$$

3. Effects of uncertainties on dimension and frequencies

Finally, the effects of the association of dimension and frequency errors were analyzed together. Assuming the uncertainties on frequency and dimension are 0.5% and 0.04 mm, respectively, 200 independent frequency realizations and 200 independent realizations of dimensions were generated from normal distributions, $\mathbf{f}^m \sim N\left(\mathbf{f}^0, (0.005\mathbf{f}^0)^2\right)$ and $\mathbf{dim}^n \sim N(\mathbf{dim}^0, 0.04^2)$. The number of random realizations was chosen following preliminary convergence tests. The stiffness constants $\mathbf{C}_{ij}^{mn}$ were then obtained by solving the inverse problem using $\mathbf{f}^m$ as proxy for experimental frequencies with errors and $\mathbf{f}^n$ calculated for the inadequate forward model : specimen of perfect RP shape with uncertain dimensions $\mathbf{dim}^n$. The mass used in the forward model is m^0 (Table I). Precisely, this is done using the objective function defined in Eq. (4). The input parameters are summarized in Fig. 8 (block D+F).

$$F(\mathbf{C}_{ij}^{mn}) = \sum_k \left(\frac{f_k^m - f_k^n(\mathbf{C}_{ij}^{mn})}{f_k^m} \right)^2 \tag{4}$$

4. Data Analysis

For the three cases described above, the error $\delta\mathbf{C}_{ij}^{est}$ is calculated for each realization of the determined stiffness constants as

$$\delta\mathbf{C}_{ij}^{est} = \frac{\mathbf{C}_{ij}^{est} - \mathbf{C}_{ij}^0}{\mathbf{C}_{ij}^0} \times 100\% \tag{5}$$

where $\mathbf{C}_{ij}^{est} = (\mathbf{C}_{ij}^p, \mathbf{C}_{ij}^q, \mathbf{C}_{ij}^{mn})$ and $\mathbf{C}_{ij}^0$ is the elasticity of the reference specimen.

B. Results

The normality of the distribution of each $\delta\mathbf{C}_{ij}^{est}$ was verified using Shapiro-Wilk's test ($p < 0.05$). Table II summarizes the distribution of $\delta\mathbf{C}_{ij}^{est}$ (Eq. (5)) and the root-mean-square error σ_f representing the quality of the frequency fit at the minimum of the objective function. The engineering moduli, including the Young's moduli (E_1 and E_3) and the Poisson's ratio (ν_{23}, ν_{31} and ν_{21}), were also compared to the reference values (obtained from $\mathbf{C}_{ij}^0$ in Table I). The errors are summarized in Table II. The 95% confidence intervals (CIs) of the errors were evaluated (Fig. 9). For case (D), (F) and (D+F), the 95% CIs were calculated as mean ± 2×SD. The values of the errors indicated in the following text correspond to the larger absolute value of the 95% CI bounds, unless otherwise stated.

Table II. The errors (mean±SD in %) on stiffness constants (Eq. (5)) and the engineering moduli due to four sources of error: uncertainties on dimension (D), on frequencies (F), on dimension and frequencies together (D+F) and imperfect specimen geometry (S) detailed in Sec. V.

Error source	D	F	D+F	S
δC_{11}	-0.41±1.51	-0.12±1.41	-0.52±1.70	3.56±1.61
δC_{33}	0.16±2.68	0.00±1.44	0.13±2.52	-2.18±1.51
δC_{13}	-0.21±1.38	-0.09±2.60	-0.36±2.16	2.22±2.08
δC_{44}	0.02±1.27	0.00±0.53	0.07±1.41	-0.52±0.91
δC_{66}	-0.01±1.10	-0.03±0.48	-0.05±1.18	0.85±0.68
δE_1	-0.16±1.08	-0.07±0.46	-0.22±1.09	1.55±0.82
δE_3	0.17±2.62	-0.00±1.09	0.20±2.67	-3.19±1.10
$\delta\nu_{23}$	0.03±1.92	-0.01±1.94	-0.06±2.68	2.78±1.15
$\delta\nu_{31}$	0.34±2.26	0.05±1.79	0.32±2.24	-2.01±1.53
$\delta\nu_{21}$	-0.50±2.06	-0.14±1.89	-0.55±2.24	2.42±1.49
σ_f	0.35±0.23	0.43±0.06	0.58±0.16	0.29±0.09

The errors caused by dimension imprecision (case (D)) and both dimension and frequency imprecision (case (D+F)) are comparable, i.e., less than 5.5% for C_{11}, C_{33} and C_{13}, less than

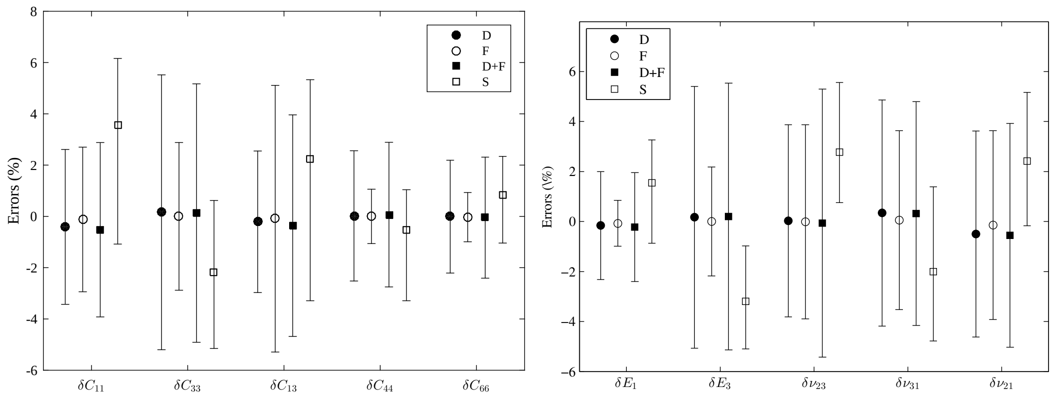

Figure 9. The mean and 95% confidence intervals of the errors on stiffness constants and engineering moduli corresponding to case (D), (F), (D+F) and (S). The error bars show the upper and lower bounds of the intervals and the mean values are represented at the center of the errorbars by the 'circle' or 'square' makers. For case (D), (F) and (D+F) the intervals were estimated as mean $\pm$ 2×SD, for case (S) they were evaluated by fitting the cumulative distribution functions of the errors using kernel density estimators.

2.9% for C_{44} and C_{66}. Similar observation also applies to the engineering moduli for which the errors are less than 2.4% for E_1, 5.5% for E_3 and 5.4% for the Poisson's ratios. Errors caused by frequency imprecision alone are less than 1.1% for C_{44} and C_{66}, 2.9% for C_{11} and C_{33} and 5.3% for C_{13}, which agrees well with the sensitivities of resonant frequencies to the stiffness constants[29]. The error δC_{13} is larger when frequencies are imprecise compared to when dimensions are imprecise. The errors on shear stiffness constants (δC_{44} and δC_{66}) are smaller than the errors on longitudinal (δC_{11} and δC_{33}) and off-diagonal stiffness constants (δC_{13}) in all the 3 cases (D, F, and D+F). Overall, δE_3 is two times larger than δE_1 and the accuracy associated to Young's moduli E_1 and E_3 are similar to that associated to C_{11} and C_{33}. For all the stiffness constants, σ_f are around 0.35%, 0.43% and 0.58% when dimension imprecision, frequency imprecision and both dimension and frequency imprecision are considered, respectively.

V. SIMULATION OF THE ERRORS DUE TO IMPERFECT SPECIMEN GEOMETRY

A. Method

In RUS, the inverse problem to determine stiffness constants is solved assuming that the specimen is a perfect RP. In this section, we investigate the uncertainty on stiffness associated to this assumption resorting to a 'virtual' RUS experiment (Fig. 8 (block S) and Fig. 10):

(1) For each of the 23 bone specimens, the resonant frequencies $\mathbf{f}^{fem}$ were calculated using the finite element method considering the actual specimen's geometry derived from SR-μCT images, measured mass m^{exp} and specimen's stiffness $\mathbf{C}_{ij}^{exp}$ determined in the usual manner assuming a perfect RP shape. Details on the finite element implementation are given in appendix (Appendix A).

(2) The stiffness constants $\mathbf{C}_{ij}^{fem}$ of each specimen were estimated solving the inverse problem defined by the frequencies $\mathbf{f}^{fem}$ (the first 40 frequencies) considered as measurements and a forward model characterized by a perfect RP geometry (dimensions $\mathbf{dim}^{exp}$) and specimen's mass (m^{exp}) (Sec. III).

These resulting $\mathbf{C}_{ij}^{fem}$ are the stiffness constants of a RP bone specimen that would exhibit the same resonant frequencies as the imperfect shape bone specimens with stiffness constants $\mathbf{C}_{ij}^{exp}$. Constants $\mathbf{C}_{ij}^{fem}$ are biased by imperfect specimen geometry and are compared to the true stiffness constants of the specimen used in the FEM model ($\mathbf{C}_{ij}^{exp}$). Namely, we calculate the errors $\delta\mathbf{C}_{ij}^{fem} = \frac{\mathbf{C}_{ij}^{fem} - \mathbf{C}_{ij}^{exp}}{\mathbf{C}_{ij}^{exp}} \times 100\%$.

B. Results

The errors on stiffness constants and the engineering moduli due to imperfect geometry of the specimens are summarized in Table II (last column). As only 23 specimens were included and the errors were not normally distributed, the 95% CIs of the errors (Table III and Fig. 9) were evaluated by fitting the cumulative distribution functions of the errors using kernel density estimators. For all the stiffness constants, there is a bias, i.e. the mean value of the errors is not zero and it can be positive or negative depending on the constant (the mean values vary from -3.19% to 3.56%). The SD of the errors varies from

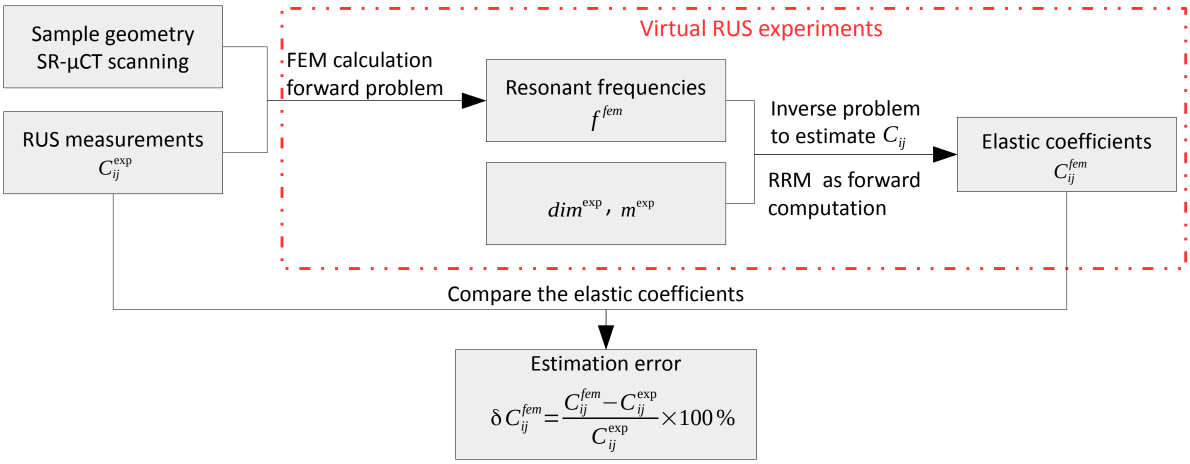

Figure 10. Diagram of the FEM simulation for quantifying the bias caused by imperfect specimen geometry. $\mathbf{C}_{ij}^{exp}$ are bone stiffness constants measured by RUS (Section III B), $\mathbf{f}^{fem}$ are the resonant frequencies calculated from the actual specimen geometry, $\mathbf{dim}^{exp}$ are the dimensions of the specimens measured by caliper, $\mathbf{C}_{ij}^{fem}$ are the stiffness constants calculated by solving the inverse problem, and $\delta\mathbf{C}_{ij}^{fem}$ represent the estimation errors.

0.68% to 2.08%. In particular, the errors on shear stiffness constants present a smaller variation than longitudinal and off-diagonal ones (see the 95% CIs in Table III) and the errors on Young's moduli present slightly less variability compared to the longitudinal stiffness constants (Table II and III).

Table III. The 95% CIs (in %) of the errors on stiffness constants and the engineering moduli due to imperfect specimen geometry.

	δC_{11}	δC_{33}	δC_{13}	δC_{44}	δC_{66}
95% CI	[-1.08, 6.16]	[-5.15, 0.62]	[-3.29, 5.33]	[-3.29, 1.04]	[-1.04, 2.34]
	δE_1	δE_3	$\delta \nu_{23}$	$\delta \nu_{31}$	$\delta \nu_{21}$
95% CI	[-0.87, 3.27]	[-5.09, -0.98]	[0.75, 5.56]	[-4.78, 1.39]	[-0.17, 5.17]

VI. DISCUSSION AND CONCLUSION

In this study, we performed simulations to quantify the errors on the stiffness constants determined from RUS measurements. We used typical elasticity values of human cortical bone as reference and studied the effects of errors due to (1) uncertainties on the measurement of frequencies; (2) uncertainties on the measurement of dimensions (assuming a perfect RP shape); (3) imperfect specimen's geometry (deviation from a perfect RP). The first two points were addressed with a calculation of error propagation with Monte-Carlo simulations which require a statistical model of the quantities investigated. For dimensions (of an assumed perfect RP) and frequencies, it is reasonable to assume normal distributions around the reference values. The third source of error is the deviation of the shape from a perfect RP. In that case we do not have a statistical model for the shape alterations, i.e., Monte-Carlo simulations cannot be used. Hence, the third point was addressed using actual experimental data on a collection of 23 bone specimens. The main parameters of the Monte-Carlo simulations were the assumed level of error on experimentally determined resonant frequencies, set to 0.5%, and experimentally determined specimen's dimensions, set to 0.04 mm (∼1%). The choice of these values is consistent with our experience of using RUS to measure bone specimens[17].

Using micro-CT, we could quantify the range of geometrical errors associated to a simple specimen's preparation procedure. We found that perpendicularity and parallelism errors were in average less than 1° and always less than 2° (Fig. 6).

Overall, we found errors on elasticity values of a few percents, or less than one percent, depending on the considered stiffness constant. Note that we discuss the accuracy errors reporting the 95% CIs of the error. Consistent with the findings of several previous studies[26,29], we found that the off-diagonal stiffness constants presented the highest errors and shear constants the smallest ones. This is related to the higher sensitivity of RUS to shear stiffness constants. Comparing the uncertainties of the sources of error (dimensions and frequencies) and the uncertainties of the errors on shear stiffness constants (the most precisely determined ones), comparable values were observed (Table II), i.e., 0.04 mm (∼1%) uncertainty on dimensions and 0.5% uncertainty on frequencies leads to ∼1.2% and ∼0.5% uncertainties on the errors of shear stiffness constants, respectively. Additional Monte-Carlo simulations, following the same routine in Section IV A showed that increasing the error level of dimensions and frequencies by 20%, i.e., the uncertainties of dimensions and frequencies became 0.05 mm and 0.6%, respectively, will increase the CIs of the error on shear stiffness by ∼16% to 25%, approximately.

For all the stiffness constants but C_{13}, dimension uncertainties lead to larger errors in elasticity compared to the case where only frequency uncertainties are considered (Table II and Fig. 9). For C_{13}, the largest error is observed for frequency uncertainties, suggesting that C_{13} may be less sensitive to dimension imperfections than to resonant frequencies in current simulation conditions. Interestingly, dimension uncertainties or a coupling of frequency and dimension uncertainties caused similar levels of errors on the stiffness constants (Table II and Fig. 9).

Deviation of the actual specimen's shape from a perfect RP affects the accuracy of the stiffness constants measured with RUS. This is because the forward model used to solve the inverse problem, assuming a perfect RP geometry, is not correct. The approach introduced in Section V aimed at simulating the effect of this source of error. It is important to note that, in general (when a micro-CT scan of the specimen is not available), only the mass can be accurately measured as opposed to the dimensions (because the geometry is in general not perfect). This is the reason why mass (m^{exp}) but not mass density was used in the simulations in Secs. IV and V. The uncertainty of the mass was about 0.1% since the precision of the balance is ± 0.1 mg and the mass of the bone specimens are around 100 mg. A linear relationship exists between mass and stiffness constants, consequently, for given dimensions and resonant frequencies[26], a mass uncertainty of 0.1% will cause the same uncertainty (0.1%) on the stiffness constants, which is negligible compared to the error levels caused by other factors. Accordingly, the uncertainty of mass was not considered in this work. We have observed that most of the caliper-measured volumes were overestimated of approximately 3% in average compared to the volumes deduced from SR-μCT images. Accordingly, the quantified elasticity errors are a result of both overestimated dimensions and irregularity of the RP shape. The elasticity errors due to an imperfect RP geometry (Table III and Fig 9) were between 2.3%∼6.2%. The comparison of the contribution of the three sources of errors to the precision of RUS measurements shows that errors due to an imperfect geometry are found to be of the same order as the errors calculated by Monte-Carlo simulations caused by frequency or dimension uncertainties in our specific case.

It is noteworthy that the values of σ_f obtained from simulations in the present study ($\sigma_f \approx 0.58\%$ with Monte-Carlo simulations and $\sigma_f \approx 0.29\%$ using FEM simulations with the imperfect shape) are similar to values reported for actual RUS measurements of bone and other attenuative materials[17,22] where σ_f is typically in the range 0.25-0.40%. This suggests that the simulations accurately reproduce the experimental error characteristic of RUS measurements. The level of errors quantified in the present study are consistent with the reported precision of RUS for human cortical bone application (3%, 5% and 0.4% for longitudinal, off-diagonal and shear stiffness constants, respectively)[17], estimated from the RMSE σ_f.

This study has introduced an original methodology to quantify errors in RUS measurements. The method was applied to bone but could be used to assess the accuracy for RUS measurements of various materials. Note that it has been possible to implement Monte-Carlo simulations only because an automated pairing of frequencies (for the calculation of the objective function) was possible. This automated pairing was initially developed to process spectra of attenuative materials where several resonant peaks can not be retrieved[34] and it is also efficient to process synthetic resonant frequencies as in the present study where no peak is missing.

In RUS measurements, specimens are assumed to be homogeneous, although cortical bone specimens are inhomogeneous to some extent. When the wavelength is much greater than the length scale of the inhomogeneity, the material can be regarded as a homogeneous material. A conservative estimation of acceptable inhomogeneity in RUS was suggested by Ulrich et.al.[28]. The maximum size of an inhomogeneity should be smaller than a threshold $\xi \leq 2l/n$, where l is the smallest dimension of the sample and n can be taken as the number of the considered resonant frequencies. Here with $l = 3\ mm$ and $n = 40$, the threshold is $\xi = 150\ \mu m$, which is larger than the diameter of the pores in human cortical bone (Haversian canals diameter is typically in the range of $20 - 100\ \mu m$). According to this criterion, bone specimens in the present work may be considered as homogeneous.

Aside of the uncertainties in the values of the inputs in RRM, including mass, dimensions and stiffness constants, the RRM has a limited accuracy associated to the truncation to M-th order of the polynomial approximation of the displacement field. Resonant frequencies calculated with RRM are more accurate with increasing values of M but as a counterpart, the computing time increases. In the present work, this was a critical issue because large numbers of iterations were involved to solve the inverse problem in the Bayesian framework. In practice, $M = 10$ used in this study, following the suggestion by Migliori and Sarrao[26], is a good compromise between accuracy and computing time if the first 50 resonant frequencies are considered. A preliminary test showed that the root-mean-square-error between the RRM-yielded frequencies when $M = 10$ and $M = 20$ is close to 0.07% for the first 40 frequencies, which is negligible compared to the magnitude of other sources of error that we handled with in this work.

This study has some limitations. We used simulated resonant frequencies as proxy for RUS data as input to the inverse problem. Precisely, the eigenfrequencies of the first forty vibration modes were used. In actual RUS experiments to measure bone, a maximum of fifteen to twenty frequencies among the first forty can actually be retrieved due to peak overlapping[22]. In theory, taking into account more frequencies should improve the precision of the determination of stiffness constants because more information is used for the inverse problem. However, in practice, the achievable precision also depends on the quality of the frequency measurement which decreases in the higer frequency range due to the increased modal density and peak overlapping. Since the resonant frequencies are much more sensitive to shear stiffness constants[39], it is expected that using less frequencies than in the present study would essentially decrease the precision of constants C_{11}, C_{33} and C_{13} but would have little impact on the precision of the shear stiffness constants. The results of the simulation in Sec. V critically rely on the actual pixel size in SR-μCT experiments, because the exact shape of the specimens were used to compute the 'true' resonant frequencies for the inverse problem. However, we did not perform calibration for identifying the actual pixel size during SR-μCT experiments. This could partly affect or bias the results. Another limitation is that we did not simulate the error on stiffness constants due to a combination of frequency uncertainty and imperfect RP geometry. In view of the results of Sec. IV, we expect that elasticity errors would only be slightly larger. Furthermore, some sources of errors in RUS have not been considered such as the effect of imperfect boundary conditions[40] and the uncertainty on the measurement of specimen's mass.

The validation of the measurement of bone elasticity with RUS relies (1) on the successful measurement of a reference transverse isotropic material with a Q-factor similar as bone's Q-factor[22]; (2) on the comparison of the stiffness constants obtained with RUS and from the independent measurement of the time-of-flight of shear and longitudinal waves in bone specimens[16,17]; and (3) on the results of the present study focused on the quantification of accuracy errors. The latter suggest that despite the typical non-perfect geometry of bone specimens and despite the relatively large uncertainty in the measurement of the bone resonance frequencies (due to attenuation), the stiffness constants are obtained with a maximum error of a few percents. A very conservative accuracy value can be quantified by the larger absolute value of the (non symetric) 95% CI bounds; accuracy defined like this was 6.2%

for longitudinal stiffness and 3.3% for shear stiffness, 5.1% for Young's moduli and 5.6% for Poisson's ratios (Table III).

To further enhance the accuracy of bone RUS measurement, possible paths would be (1) using a specific implementation of the Rayleigh-Ritz method for nonrectangular parallelepiped specimen[29], provided that the angles between the specimen's surfaces can be measured; (2) decreasing the frequency uncertainty by improving the signal processing of RUS spectra.

ACKNOWLEDGMENTS

This work has received financial support from the Agency National Research under the ANR-13-BS09-0006 MULTIPS and ANR-14-CE35-0030-01 TaCo-Sound projects and was done in the framework of LabEx PRIMES (ANR-11-LABX-0063) of Université de Lyon. The authors would like to thank Rémy Gauthier, Hélène Follet and David Mitton for the collection of bone specimens and the help in conducting SR-μCT imaging experiments. The authors wish to acknowledge Didier Cassereau for providing technical support with numerical computations and Pascal Dargent for designing the setup and the protocol of bone specimen preparation, as well as the ESRF for providing beamtime through the experiment MD927 and Lukas Helfen for his assistance in image acquisition on beamline ID19.

Appendix A: Calculation of resonant frequencies using Finite element modeling (FEM)

Bone was modeled as a homogeneous transversely isotropic material. The bone volumes obtained from the SR-μCT were discretized into about 3 million quadratic tetrahedral elements. This corresponded to a maximum element size of 0.12 mm, which was chosen after a convergence study and ensures at least 10 elements per smallest wavelength in the investigated frequency bandwidth. A modal analysis was conducted to calculate the eigenfrequencies. We used the software Code-Aster (ver 12.5, EDF R&D, France, license GNU GPL, http://www.code-aster.org).

The accuracy of the finite element model was evaluated by comparing the first 40 FEM eigeinfrequencies to eigenfrequencies calculated with the Rayleigh-Ritz method for a perfect

RP bone specimen (Table I). The RMSE σ_f between eigenfrequencies calculated by the two methods was $\sim 0.06\%$. After solving the inverse problem using FEM eigenfrequencies, the errors in the stiffness constants were $\sim 0.05\%$, 0.60% and 0.30% on shear, longitudinal and off-diagonal stiffness constants. These errors are at least one order of magnitude smaller than the errors related to shape imperfections (Sec. V).

REFERENCES

[1] J. Klein-Nulend, P. J. Nijweide, and E. H. Burger, "Osteocyte and bone structure," Current osteoporosis reports **1**, 5–10 (2003).

[2] P. Fratzl and R. Weinkamer, "Natures hierarchical materials," Progress in Materials Science **52**, 1263–1334 (2007).

[3] J.-Y. Rho, L. Kuhn-Spearing, and P. Zioupos, "Mechanical properties and the hierarchical structure of bone," Medical engineering & physics **20**, 92–102 (1998).

[4] Q. Grimal, K. Raum, A. Gerisch, and P. Laugier, "A determination of the minimum sizes of representative volume elements for the prediction of cortical bone elastic properties," Biomechanics and modeling in mechanobiology **10**, 925–937 (2011).

[5] J. D. Currey, *Bones: structure and mechanics* (Princeton university press, Princeton, 2002), pp. 436.

[6] D. Rohrbach, Q. Grimal, P. Varga, F. Peyrin, M. Langer, P. Laugier, and K. Raum, "Distribution of mesoscale elastic properties and mass density in the human femoral shaft," Connective tissue research **56**, 120–132 (2015).

[7] S. B. Lang, "Elastic coefficients of animal bone," Science **165**, 287–288 (1969).

[8] J. L. Katz and H. S. Yoon, "The structure and anisotropic mechanical properties of bone," IEEE Trans. Biomed. Eng. **BME-31**, 878 –884 (1984).

[9] R. Ashman, J. Rho, and C. Turner, "Anatomical variation of orthotropic elastic moduli of the proximal human tibia," Journal of biomechanics **22**, 895–900 (1989).

[10] J. Y. Rho, "An ultrasonic method for measuring the elastic properties of human tibial cortical and cancellous bone." Ultrasonics **34**, 777–783 (1996).

[11] C. Schwartz-Dabney and P. Dechow, "Accuracy of elastic property measurement in mandibular cortical bone is improved by using cylindrical specimens," Journal of biomechanical engineering **124**, 714–723 (2002).

[12]A. A. E. Orías, J. M. Deuerling, M. D. Landrigan, J. E. Renaud, and R. K. Roeder, "Anatomic variation in the elastic anisotropy of cortical bone tissue in the human femur," Journal of the mechanical behavior of biomedical materials **2**, 255–263 (2009).

[13]M. Granke, Q. Grimal, A. Saed, P. Nauleau, F. Peyrin, and P. Laugier, "Change in porosity is the major determinant of the variation of cortical bone elasticity at the millimeter scale in aged women," Bone **49**, 1020–1026 (2011).

[14]E. Lefèvre, P. Lasaygues, C. Baron, C. Payan, F. Launay, H. Follet, and M. Pithioux, "Analyzing the anisotropic hooke s law for children s cortical bone," Journal of the mechanical behavior of biomedical materials **49**, 370–377 (2015).

[15]R. G. Leisure and F. Willis, "Resonant ultrasound spectroscopy," Journal of Physics: Condensed Matter **9**, 6001 (1997).

[16]L. Peralta, X. Cai, P. Laugier, and Q. Grimal, "A critical assessment of the in-vitro measurement of cortical bone stiffness with ultrasound." Ultrasonics **80**, 119–126 (2017).

[17]S. Bernard, Q. Grimal, and P. Laugier, "Accurate measurement of cortical bone elasticity tensor with resonant ultrasound spectroscopy," Journal of the mechanical behavior of biomedical materials **18**, 12–19 (2013).

[18]T. Delaunay, E. L. Clezio, M. Guennou, H. Dammak, M. P. Thi, and G. Feuillard, "Full tensorial characterization of pzn-12%pt single crystal by resonant ultrasound spectroscopy," and Frequency Control IEEE Transactions on Ultrasonics, Ferroelectrics **55**, 476–488 (2008).

[19]R. Schwarz and J. Vuorinen, "Resonant ultrasound spectroscopy: applications, current status and limitations," Journal of Alloys and Compounds **310**, 243–250 (2000).

[20]W. H. Wang, "The elastic properties, elastic models and elastic perspectives of metallic glasses," Progress in Materials Science **57**, 487–656 (2012).

[21]H. Ledbetter, C. Fortunko, and P. Heyliger, "Orthotropic elastic constants of a boron-aluminum fiber-reinforced composite: An acoustic-resonance-spectroscopy study," Journal of Applied Physics **78**, 1542–1546 (1995).

[22]S. Bernard, Q. Grimal, and P. Laugier, "Resonant ultrasound spectroscopy for viscoelastic characterization of anisotropic attenuative solid materials," The Journal of the Acoustical Society of America **135**, 2601–2613 (2014).

[23]R. Longo, T. Delaunay, D. Laux, M. El Mouridi, O. Arnould, and E. Le Clezio, "Wood elastic characterization from a single sample by resonant ultrasound spectroscopy," Ultra-

sonics **52**, 971–974 (2012).

[24]T. Lee, R. S. Lakes, and A. Lal, "Investigation of bovine bone by resonant ultrasound spectroscopy and transmission ultrasound," Biomechan. Model. Mechanobiol. **1**, 165–175 (2002).

[25]J. H. Kinney, J. R. Gladden, G. W. Marshall, S. J. Marshall, J. H. So, and J. D. Maynard, "Resonant ultrasound spectroscopy measurements of the elastic constants of human dentin." J Biomech **37**, 437–441 (2004).

[26]A. Migliori and J. L. Sarrao, *Resonant Ultrasound Spectroscopy* (Wiley, New York, 1997), pp. 202.

[27]A. Migliori and J. D. Maynard, "Implementation of a modern resonant ultrasound spectroscopy system for the measurement of the elastic moduli of small solid specimens," Rev. Sci. Instrum. **76**, 121301 (2005).

[28]T. J. Ulrich, K. McCall, and R. Guyer, "Determination of elastic moduli of rock samples using resonant ultrasound spectroscopy," The Journal of the Acoustical Society of America **111**, 1667–1674 (2002).

[29]M. Landa, P. Sedlák, H. Seiner, L. Heller, L. Bicanová, P. Šittner, and V. Novák, "Modal resonant ultrasound spectroscopy for ferroelastics," Appl. Phys., A **96**, 557–567 (2009).

[30]P. Sedlák, H. Seiner, J. Zídek, M. Janovská, and M. Landa, "Determination of all 21 independent elastic coefficients of generally anisotropic solids by resonant ultrasound spectroscopy: Benchmark examples," Experimental Mechanics **54**, 1073–1085 (2014).

[31]A. Migliori, J. L. Sarrao, W. M. Visscher, T. M. Bell, M. Lei, Z. Fisk, and R. G. Leisure, "Resonant ultrasound spectroscopic techniques for measurement of the elastic moduli of solids," Physica B **183**, 1 – 24 (1993).

[32]A. Lebedev, L. Ostrovskii, A. Sutin, I. Soustova, and P. Johnson, "Resonant acoustic spectroscopy at low q factors," Acoustical Physics **49**, 81–87 (2003).

[33]S. Bernard, J. Schneider, P. Varga, P. Laugier, K. Raum, and Q. Grimal, "Elasticity-density and viscoelasticity-density relationships at the tibia mid-diaphysis assessed from resonant ultrasound spectroscopy measurements." Biomech Model Mechanobiol **15**, 97–109 (2016).

[34]S. Bernard, G. Marrelec, P. Laugier, and Q. Grimal, "Bayesian normal modes identification and estimation of elastic coefficients in resonant ultrasound spectroscopy," Inverse Problems **31**, 065010 (2015).

[35]H. S. Yoon and J. L. Katz, "Ultrasonic wave propagation in human cortical boneii. measurements of elastic properties and microhardness," Journal of biomechanics **9**, 459–464 (1976).

[36]M. Salomé, F. Peyrin, P. Cloetens, C. Odet, A. M. Laval-Jeantet, J. Baruchel, and P. Spanne, "A synchrotron radiation microtomography system for the analysis of trabecular bone samples," Medical Physics **26**, 2194–2204 (1999).

[37]T. Weitkamp, P. Tafforeau, E. Boller, P. Cloetens, J.-P. Valade, P. Bernard, F. Peyrin, W. Ludwig, L. Helfen, and J. Baruchel, "Status and evolution of the esrf beamline id19," in *X-ray Optics and Microanalysis: Proceedings of the 20th International Congress*, Vol. 1221 (2010) pp. 33–38.

[38]G. Anderson, "Error propagation by the monte carlo method in geochemical calculations," Geochimica et Cosmochimica Acta **40**, 1533–1538 (1976).

[39]B. J. Zadler, J. H. Le Rousseau, J. A. Scales, and M. L. Smith, "Resonant ultrasound spectroscopy: theory and application," Geophysical Journal International **156**, 154–169 (2004).

[40]A. Yoneda, "Intrinsic eigenvibration frequency in the resonant ultrasound spectroscopy," Earth, planets and space **54**, 763–770 (2002).